Taylor & Francis
Taylor & Francis Group

Science and Technology of Welding and Joining

ISSN: (Print) (Online) Journal homepage: https://www.tandfonline.com/loi/ystw20

Effect of tool offsetting on friction stir welding of dissimilar aluminium matrix composite and aluminium alloy

Chen Wang, Beibei Wang, Peng Xue, Dingrui Ni, Bolv Xiao, XiaoDong Hou, Jianbo Gao, Liqing Chen & Zongyi Ma

To cite this article: Chen Wang, Beibei Wang, Peng Xue, Dingrui Ni, Bolv Xiao, XiaoDong Hou, Jianbo Gao, Liqing Chen & Zongyi Ma (2022) Effect of tool offsetting on friction stir welding of dissimilar aluminium matrix composite and aluminium alloy, Science and Technology of Welding and Joining, 27:7, 586-593, DOI: 10.1080/13621718.2022.2091342

To link to this article: https://doi.org/10.1080/13621718.2022.2091342

View supplementary material

Published online: 27 Jun 2022.

Submit your article to this journal

Article views: 199

View related articles

View Crossmark data

Full Terms & Conditions of access and use can be found at
https://www.tandfonline.com/action/journalInformation?journalCode=ystw20

SCIENCE AND TECHNOLOGY OF WELDING AND JOINING
2022, VOL. 27, NO. 7, 586–593
https://doi.org/10.1080/13621718.2022.2091342

Effect of tool offsetting on friction stir welding of dissimilar aluminium matrix composite and aluminium alloy

Chen Wang[a,d], Beibei Wang[a,b], Peng Xue[b], Dingrui Ni[b], Bolv Xiao[b], XiaoDong Hou[a], Jianbo Gao[a], Liqing Chen[c] and Zongyi Ma[b]

[a]Centre of Excellence for Advanced Materials, Dongguan, People's Republic of China; [b]Shi-changxu Innovation Center for Advanced Materials, Institute of Metal Research, Chinese Academy of Sciences, Shenyang, People's Republic of China; [c]State Key Laboratory of Rolling and Automation, Northeastern University, Shenyang, People's Republic of China; [d]Spallation Neutron Source Science Center, Dongguan, People's Republic of China

ABSTRACT
Commercial 6061 Al alloy and SiCp reinforced 6092 Al matrix composite (AMC) were joined by friction-stir welding (FSW) with different tool offsets. Results show offsetting the pin to Al alloy side could significantly reduce tool wear, while maintaining ultimate tensile strength of the joint around 180 MPa. As tool offset increased from zero to 3 mm, pin and shoulder wear length reduced from 0.17 mm to almost zero and from 0.28 to 0.02 mm, respectively. The corresponding estimated maximum safe welding length increased from 568 to 3125 mm. Fe debris were generated from the steel pin by the sharp SiC particles, then transferred into the nugget zone, eventually formed Al8Fe2Si particles during the FSW process.

ARTICLE HISTORY
Received 2 March 2022
Revised 6 June 2022
Accepted 10 June 2022

KEYWORDS
Dissimilar friction stir welding; tool wear; particle reinforced Al matrix composite; Al alloy; pin offset

Introduction

Ceramic particles discontinuously reinforced Al matrix composites (AMC) are often used in aerospace and automotive industries due to its high modulus, high strength, low thermal expansion coefficient, and good thermal conductivity [1,2]. These physical and mechanical properties have attracted considerable attention; however, high cost and poor ductility limited their wide use in the industrial application. It is often the case that key parts are made of AMC, but commercial Al alloys are still used for the main product especially in aerospace and automotive industries. Therefore, it is necessary to join AMC with commercial Al alloys as a solution to reduce cost and improve performance.

Fusion welding is traditionally used to join AMC parts, but this technique often generates large porosity and deleterious reactions between the reinforcement particles and liquid Al matrix in the fusion zone, causing mechanical degradation of AMC joints [3,4]. Friction stir welding (FSW) was first developed by The Welding Institute (TWI) in 1991 as an innovative solid state welding technique, to avoid these drawbacks arose from conventional fusion welding methods [5]. Since then, FSW has been successfully used to join Al alloys by industrial manufacturers, and achieved high quality joints between Al alloys and other materials (referred as 'dissimilar FSW' in this study), including Al alloys and Mg alloys, Al alloys and Cu alloys, and Al alloys and steels [6–9]. Theoretically, a high-quality joint is more likely to be achieved between Al alloys and its corresponding AMC due to their similar properties.

Indeed, several researchers have already worked on the dissimilar FSW between AMC and Al alloys [10–14]. It was found that welding parameters are the dominant factors affecting the quality of the dissimilar FSW joints. Optimised welding parameters (including rotation rate and traverse speed) can be obtained through experiments to produce high quality joints [15–17]. It was also found that the relative position of raw materials in respect with the welding direction, often referred as the advancing side (AS) or retreating side (RS), can play a critical role in the FSW process. Wert [10] studied the influence of raw material position on the mixing effect between 20vol.-%Al_2O_3/2014Al composite and 2014 Al alloy by FSW, and they found that the mixing effect was improved when using 20vol.-%Al_2O_3/2014Al composite on the AS and the 2014 Al alloy on the RS. However, Guo et al. [11] suggested to put 6063 Al on the AS and B4Cp/1100Al composite on the RS, in order to get a better mixing effect and a stronger joint. In general, the strength of FSW

CONTACT Peng Xue pxue@imr.ac.cn Shi-changxu Innovation Center for Advanced Materials, Institute of Metal Research, Chinese Academy of Sciences, 72 Wenhua Road, Shenyang 110016, People's Republic of China; Xiaodong Hou xiaodong.hou@ceamat.com Centre of Excellence for Advanced Materials, 4 Qinyuan Road, Dongguan 523808, People's Republic of China

Supplemental data for this article can be accessed here. https://doi.org/10.1080/13621718.2022.2091342

© 2022 Institute of Materials, Minerals and Mining. Published by Taylor & Francis on behalf of the Institute.

joints is considered as the key factor for determining the sample position arrangement. The mixing effect of the FSW joint between AMC and Al alloys is considered to be better when the harder material is located on the AS [11].

In addition to the welding parameters, tool wear also needs to be considered for dissimilar FSW of AMC and Al alloys, because of the existence of hard particles in the AMC. Steel tools are often used in FSW, but they show serious wear after a short time of welding. It is often the case that the tool wear was too serious to accomplish a long distance welding. Moreover, wear debris generated from the tool wear and related reactants may reduce the overall mechanical performance of the joints. Feng et al. [18] reported that the formation of the deleterious phase Cu2FeAl7 resulted in a decrease in the joint strength during the FSW of SiCp/2009Al composites.

Various methods were developed to increase the lifetime of steel tools in FSW. It was found that the tool wear rate could be reduced by increasing rotation rate and decreasing traverse speed [19–21]. It was also reported that offsetting the tool to the Al alloy side could reduce the tool wear during FSW of Al–steel and Al–Cu systems [22–24], but not proved in the AMC-Al alloy combination. Cioffi et al. [12] studied the mixing effect of tool offset between AMC and Al alloy without considering the tool wear. They found severer material flow by offsetting the tool to Al alloy, causing a weak bonding in the bottom of joint. They also studied the effect of offsetting to the AMC side and found a weak joint due to bad material flow. However, Xiao et al. [13] reported that more Al alloy was likely to be introduced into the nugget zone (NZ) when offsetting the tool towards the Al alloy side, forming a weak Al layer.

In this study, the tool wear behaviour caused by tool offsetting during the dissimilar FSW of AMC and Al alloy was studied for the first time. The microstructures, hardness profiles and tensile properties of FSW joints were carefully investigated to understand the impact of offsetting the tool to the Al alloy side and elucidate wear mechanism with practical implication for a wide application of this method.

Experimental

Two base materials (BMs), 17 vol.-% SiCp/6092Al composite rolled plate (referred as AMC plate in this study) and commercial 6061Al-T651 alloy rolled plate (referred as Al alloy plate in this study), were obtained with a dimension of 300 mm × 80 mm × 6 mm for friction stir butt welding along the rolling direction. The chemical compositions of Al matrix in AMC and Al alloy are shown in Table S1. Before welding, the AMC plates were solution treated at 530°C for 1 h and then quenched in water at room temperature, followed by immediate subsequent artificial aging treatment at 175°C for 4 h. The tensile properties of the BM plates perpendicular to the rolling direction are listed in Table S2.

The AMC plate was located on the AS and the Al alloy plate was located on the RS during welding. The cylindrical thread pin and concave shoulder were both made of H13 steel, using a design that the pin and the shoulder could be easily separated for wear assessment by loosening the side screw, as schematically illustrated in Figure 1(a). The shoulder diameter was 20 mm and the pin diameter was 6 mm. The pin length was 5.75 mm measured when the shoulder and pin assembled together, referred as ‘effective pin length’ in the following discussions. The rotation rate was chosen as 1000 rev min^{-1} and the traverse speed was set to 50 mm min^{-1} to achieve maximum wear [19]. The welding length was 250 mm and the offset values to the Al alloy side were set as 0, 1, 2 and 3 mm (referred as FSW-0, FSW-1, FSW-2, FSW-3 in the following discussions). The schematic illustration of the FSW experimental design is shown in Figure 1(b).

The tool wear was assessed by weighing the pin and shoulder using a top pan balance before and after welding. The pin and shoulder length were measured by vernier calliper. The cross-section of the joint perpendicular to the welding direction was imaged using an optical microscope (OM). The particles inside the NZ were examined by using TECNAI G2 F20 transmission electron microscopy (TEM), equipped with an energy disperse spectroscopy (EDS) system. The samples were first mechanically ground to a thickness of 50 μm and then punched into discs of 3 mm diameter. The discs were dimpled and ion-milled at about −70°C before TEM observation.

The microhardness profiles of the welds were measured on the cross-section along the centre line across the welded plates using a Vickers hardness tester using 500 gf measurement load for 15 s. Tensile specimens with a dimension of 40 mm × 10 mm × 6 mm were prepared for examining tensile properties of FSW joints, obtained perpendicular to the welding direction with the NZ at the gauge centre. In order to investigate the local mechanical behaviour near the welding line, mini-size dog-bone shaped tensile specimens with a dimension of 5 mm × 1.4 mm × 1.0 mm were also prepared perpendicular to the FSW direction with the interface of Al alloy and AMC at the gauge centre, using an electrical discharge machine (see Figure 1(c)). Tensile tests for large and mini tensile specimens were conducted at an initial strain rate of 1×10^{-3} s^{-1}, using Instron 5982 tensile testing machine and Instron 5848 tensile testing machine, respectively; representative tensile results were obtained by averaging at least three repeated experiments for each sample type.

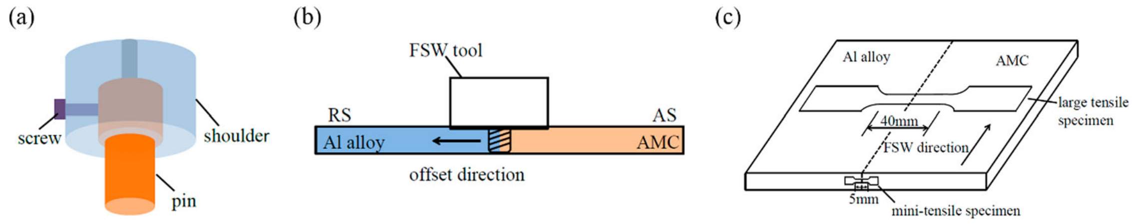

Figure 1. Schematic illustration of (a) dissimilar FSW of AMC and Al alloy (b) the location of the tensile specimen.

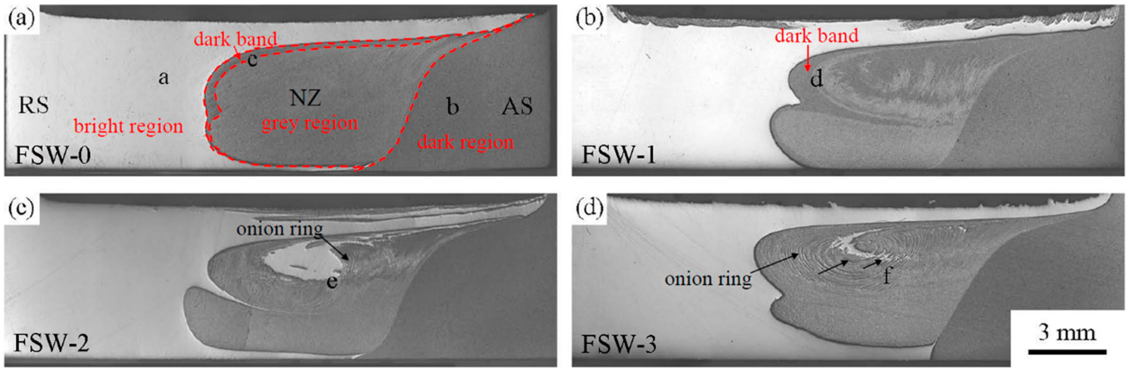

Figure 2. Cross-sectional macrostructure of dissimilar FSW joint between AMC and Al alloy with different pin offset to 6061 Al alloy side.

Results and discussion

The optical microscope images in Figure 2 show macrostructures of the weld cross-section perpendicular to the welding direction with different tool offsets, where no macroscopic defects were found in the welded joint of the four FSW samples. The dark region is AMC, the bright region is Al alloy, and the grey region is the mixing zone in all four samples. SiC particles were found uniformly distributed in the grey region of FSW-0 sample except the dark band in the upper boundary of NZ as shown in Figure 2(a). It was also confirmed offsetting the tool to the Al alloy side could significantly change the NZ morphology (see Figure 2(b–d)). With increasing the offset value, the grey region is becoming brighter and less uniform, indicating that SiC particles are reduced due to the lack of feeding from the AS side. The separation of the NZ along the vertical direction was observed with offset to Al alloy side, showing that an 'ϵ-shape' caused by complex flow of the NZ was made up with horizontal fluxion and vertical fluxion [25]. The AMC involved in the flow were reduced with the tool offset to Al alloy side, hence the mixing effect between AMC and Al alloy seemed to be inadequate in the vertical direction, resulting in the layer separation of NZ.

More details of the welding microstructures corresponding to the labelled areas (a–f) in Figure 2 are shown in Figure 3, obtained using a higher magnification OM. Only a small quantity of impurity was found in the Al alloy of FSW-0 sample, while dense SiC particles were uniformly distributed in the AMC matrix (see Figure 3(a,b)). Figure 3c shows microstructures of the dark band in NZ upper boundary. The characteristic of SiC particles distribution in the dark band was similar to that in the AMC BM, due to insufficient mixing and mutual diffusion as the AMC was brought into the NZ. Similar dark bands were also found in the FSW-1 sample as shown in Figures 2(b) and 3(d), then gradually evolving into an onion-ring structure when further increasing the offset values in FSW-2 and FSW-3 samples as shown in Figures 2(c,d) and 3(e,f). Bright bands in the onion-ring structure are Al alloy with few SiC particles while the dark bands are AMC or SiC particle enriched Al alloy, caused by excess Al alloy being brought into the NZ due to offsetting and the unique stirring mechanism of FSW.

The original shape of a typical pin before welding is illustrated in Figure 4(a). For each sample, a new pin was used and the morphologies of the pin after a 250 mm welding distance are shown in Figure 4(b–d) to investigate the influence of tool offsetting. Obvious wear was found in the pins used for FSW-0 and FSW-1 samples, as the pin threads almost disappeared. The middle part of the pin underwent most serious wear as compared with top and root parts. This self-optimised morphology was also reported in other studies [19–21] and suggested to use this special profile as a novel shape design to reduce pin wear. However, in term of tool morphology, hardly any wear was observed in FSW-2 and FSW-3 samples. This is due to the reduction of SiC particles as Al alloy volume fraction increased in NZ. In addition, no obvious changes in diameter and length were observed in these two pins, but it is believed that wear still occurred at smaller length scales.

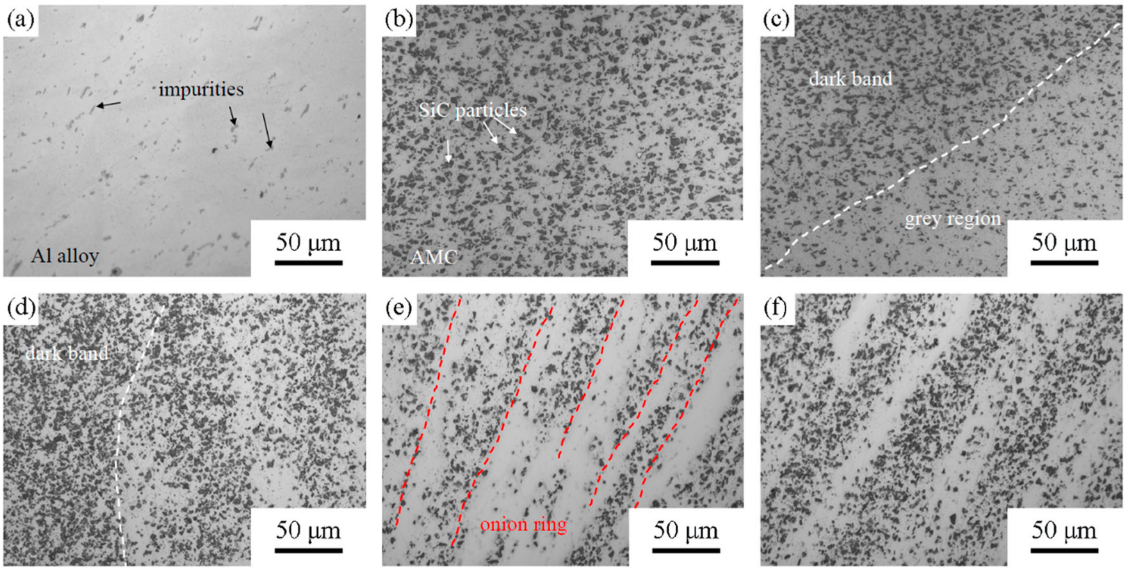

Figure 3. Optical microstructure of dissimilar FSW joint between AMC and Al alloy with different pin offset to Al alloy side (Figures (a)–(f) corresponded to the regions a–f in Figure 2).

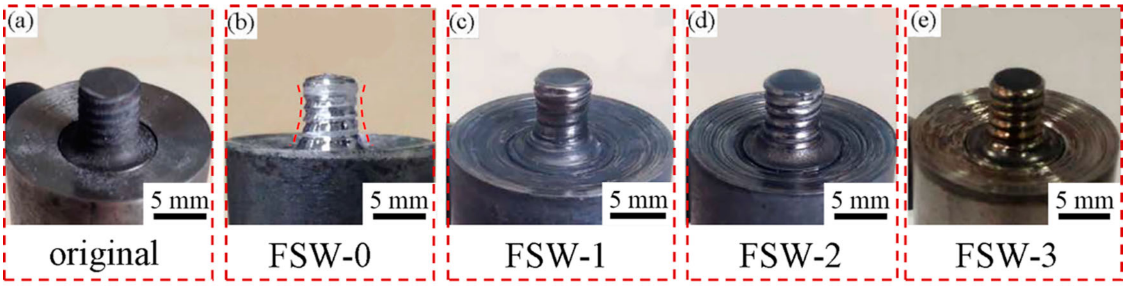

Figure 4. Morphologies of tools before and after FSW with different pin offset to Al alloy side: (a) before FSW; (b) FSW-0 sample; (c) FSW-1 sample; (d) FSW-2 sample; (e) FSW-3 sample.

To evaluate the tool wear accurately, the mass and length of all pins and shoulders were carefully measured before and after 250 mm welding, and the difference was taken as wear length and wear mass as summarised in Figure 5, showing a clear reduction trend when offset values increased from 0 to 3 mm. The wear length of the pin reduced from 0.17 mm to almost zero and the corresponding wear mass reduced from 0.18 to 0.04 g, while the wear length of the shoulder reduced from 0.28 to 0.02 mm and the corresponding wear mass reduced from 0.18 to 0.04 g and from 0.41 to 0.04 g. It is important to point out that more wear was found in the shoulder than in the pin itself for all the four samples, as pin wear length for FSW-2 and FSW-3 is almost getting to zero but the shoulder continued to get shorter. This means the shoulder is wearing more than the pin and the effective pin length is becoming relatively longer during the welding especially for large offset values (see Figure S1). As the effective pin length is becoming comparable with the rolling plate thickness (6 mm in this study) or even longer, the pin will be in direct contact with the baseplate made of steel, causing unexpected damage and poor welds. The concave shape of the shoulder helped this process as the contact between the shoulder and the plates is a ring contact with material flow inside, likely to experience a higher pressure hence causing a more rapid wear. Therefore, it is important to establish a method for calculation of allowed pin length by considering the wear of both pin and shoulder, especially for FSW with significant offsetting towards Al alloy.

The pin wear length, Δl_p, is defined in Equation (1)

$$\Delta l_p = l_p' - l_p \tag{1}$$

where l_p and l'_p are the length from the root of concave cavity of shoulder to the bottom of pin before and after FSW (schematically illustrated in Figure S1), measured when the shoulder and pin are separated. The shoulder wear length, $\Delta l s$, can be obtained by Equation (2)

$$\Delta l_s = l_s' - l_s \tag{2}$$

where l_s and l'_s are the depth in the concave cavity of the shoulder before and after FSW, respectively. Therefore, the effective pin length, Δl_{ep}, can be expressed by Equation (3),

$$\Delta l_{ep} = l_{ep}' - l_{ep} = \Delta l_p - \Delta l_s \tag{3}$$

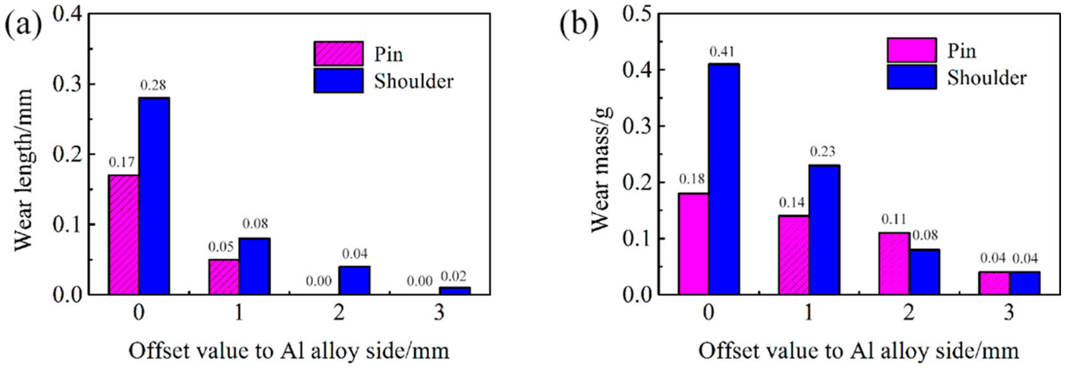

Figure 5. Tool wear after FSW with different pin offset to Al alloy side: (a) wear length; (b) wear mass.

where l_{ep} and l'_{ep} are the perpendicular distance from the shoulder bottom surface to the pin bottom surface before and after FSW, measured when the shoulder and pin are assembled together.

Based on the experimental results obtained in this study, the effective pin length changing rate is calculated as the effective pin length change (Δl_p) divided by the welding length. For FSW-0 sample, Δl_{ep} is 0.11 mm and the welding length is 250 mm, hence the effective pin length changing rate is calculated as 4.4×10^{-4}. Considering the thickness of the rolling plate is only 6 mm, it is estimated the maximum safe welding length is (6–5.75) mm / $4.4 \times 10^{-4} = 568$ mm. Applying the same calculations for other three samples, the effective pin length changing rate for FSW-1, FSW-2 and FSW-3 samples are 1.2×10^{-4}, 1.6×10^{-4} and 8×10^{-5}; the corresponding maximum safe welding lengths are estimated as 2083, 1562, 3125 mm, respectively. It is strongly recommended that this kind of calculation should be carried out for FSW to improve experimental design especially with offsetting towards Al alloys side.

Vickers microhardness distributions across the joint in Figure 6 show deviating from the traditional 'W-shape', largely due to the different mechanical properties of the two BMs. The lowest microhardness on the RS is about 54 HV (roughly 63% of Al alloy BM), while the lowest microhardness on the AS is about 80 HV (only 55% of AMC BM). It was also found that the HAZ range in the Al alloy side and the AMC side was quite different, and the width was estimated as 16 and 20 mm respectively. The hardness reduction in HAZ is directly related to the β'' phase coarsening through the thermal cycle in the FSW processing [26]. These microhardness results in Figure 6 also show that microhardness reduction in proportion to the original BM hardness on the AS is more significant than that on the RS. This is because that AMC is more likely to be affected by the thermal cycle during the FSW process than Al alloy under the same welding conditions. The mismatch between SiC particles and matrix in AMC could cause high dislocation density near the interface, contributing to the acceleration of the diffusion between Mg and Si solutes. As a result, the coarsening

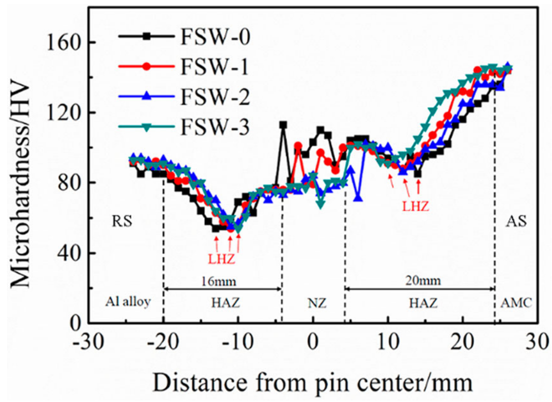

Figure 6. Microhardness profiles of dissimilar FSW joints with different pin offset to Al alloy side.

process of precipitates in the matrix will be promoted, leading to more serious hardness loss in the HAZ in AMC [27]. It is worth pointing out that the low hardness zone (LHZ) within the HAZ is closer to NZ as the pin offset increased from 0 to 3 mm, affected by the reduction of friction heat between stirring tool and SiC particles. Compared to HAZ, more fluctuations were found in the hardness profiles of NZ in all samples. The microhardness value in NZ was mainly influenced by SiC particle distribution; local regions with dense particles could show significant increase in hardness as compared to the adjacent region in FSW-0 and FSW-1 samples. The hardness distribution profile of sample FSW-3 was found more smooth, implying a more homogenous distribution of SiC particles.

The engineering stress–strain curves obtained from the FSW samples are shown in Figure 7(a). All the four samples showed similar yield strength (YS) and ultimate tensile strength (UTS), about two-thirds of 6061 Al alloy BM (see Table S2). It was found that fracture happened within the HAZ of Al alloy side in all the four samples, in particular, near the LHZ, leading to relatively low elongation (El). This is expected as the UTS of 6061 Al alloy is much lower than the that of AMC; actually, the UTS of Al alloy is even lower that the YS of AMC, hence the deformation would always happen at the Al alloy side. It was also found in these samples with

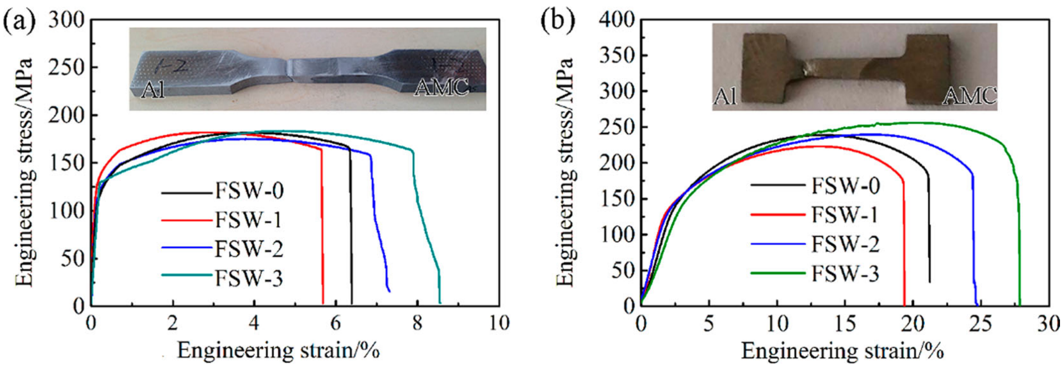

Figure 7. Engineering stress–strain curves of (a) dissimilar FSW joints; (b) mini specimens including interface between AMC and Al alloy with different pin offset.

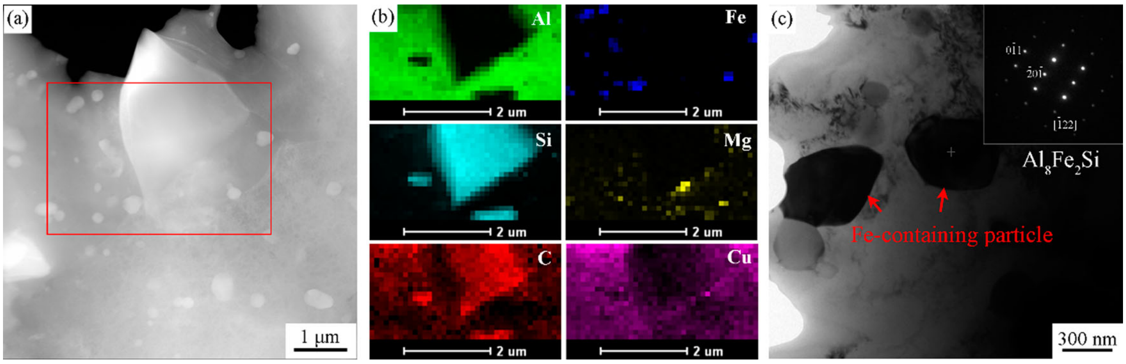

Figure 8. TEM images of (a) particles in the NZ of sample FSW-0; (b) elements distribution in the zone framed by red rectangle in (a); (c) Fe-containing particles with inserted micrographs, showing a selected area diffraction pattern.

standard dimensions that the tool offset did not have a significant influence on the tensile performance of the joints.

In order to further investigate the influence of different welding parameters on the mechanical performance, mini tensile specimens with a length of only 5 mm were prepared as shown in Figure 1(b), to exclude the HAZ influence. The engineering stress–strain curves of the four samples are shown in Figure 7(b), obtained from mini tensile specimens. The UTS of all the mini-specimens is among 220–250 MPa, still lower than the Al alloy BM but much improved than the UTS obtained from the FSW joints. All the mini specimens still fractured at the Al alloy side, suggesting the excellent interface strength between the Al alloy and AMC. Different Els were found in these mini specimens, probably caused by the different percentages of AMC and Al alloy from the irregular interface shape. Nevertheless, these tensile results strongly confirm that sound joints between these two dissimilar materials could be achieved by FSW.

The microstructure in NZ of sample FSW-0 was examined using TEM equipped with EDS (Figure 8). TEM examinations revealed many round particles with diameter around 1 μm, randomly distributed within the matrix; bigger particles with irregular shape and sharp corners were also found (Figure 8(a)). EDS mapping shows that these big particles contain mainly Si and C and round smaller particles contain mainly Fe and Al, indicating these SiC particles and the round small particles are compound formed by the chemical reaction between the Al matrix and Fe debris from stir tool (Figure 8(b)). These Fe-containing particles were further identified as Al_8Fe_2Si phase according to the analysis of the selected area diffraction pattern (Figure 8(c)). It is reported that Al–Fe–Si phase could be formed in Al alloy or AMC with high Si content, when reacted with Fe-rich material [28,29]. For example, Nazari and Shabestari [28] found the formation of Al_8Fe_2Si phase in immersion experiments between H13 steel and A380 Al alloy at a temperature of 680°C for the duration time of 2 min to 2.5 h. Besides, Al_8Fe_2Si phase could nucleate in the solidification process of high Fe containing Al–Si–Cu alloys [29].

During the FSW process, hard SiC particles with sharp corners can cause severe tool wear, transferring Fe debris from the tool into the NZ. Although the average Fe concentration is still low, there are always local regions containing high Fe concentration. The FSW process also causes a temperature increase around the pin, high enough to promote the element reaction and even melt the local Al matrix [30]. FSW process can also cause intense plastic deformation and material mixing with a strain rate of 10^0–10^2 s^{-1} and a strain of up to ∼40, and thus significantly accelerate diffusion rate and shortened diffusion distance [31–33]. In combination of all these factors, it is reasonable to expect that Al_8Fe_2Si phase could be formed by the chemical reaction between Fe debris and Al matrix within the timescale of FSW.

The above results and discussions confirm that offsetting the FSW tool to Al alloy side is a promising method to reduce tool wear, while still maintaining good mechanical performance of the welded joint between Al alloy and AMC. Experimental evidences in this study clearly show that larger offset values can increase lifetime of the pin and shoulder, with the potential to be widely applied in all the FSW between dissimilar welding materials. During the FSW process, the SiC particles with sharp corners seem to have a large impact on the tool wear, by transferring Fe debris from the tool into the NZ to form Al–Fe–Si phase. The role of Al–Fe–Si phase is still not clear; it is possible that these submicron particles could lead to dispersion strengthening of the NZ, which needs to be further investigated in the future work.

Conclusion

In this study, FSW was successfully used to join 6061 Al alloy and SiCp/6092Al composite. It was found that offsetting the tool to the Al alloy side could significantly reduce the tool wear, while maintaining good mechanical performance of the joint. The following conclusions can be made:

(1) As the tool offset values increased from 0 to 3 mm, the pin wear length reduced from 0.17 mm to almost zero and the corresponding wear mass reduced from 0.18 to 0.04 g, while the shoulder wear length reduced from 0.28 to 0.02 mm and the corresponding wear mass reduced from 0.41 to 0.04 g.
(2) The NZ shape and size largely remained unchanged even when the pin was totally off-located to the Al alloy side, but redistribution of SiC particles inside the NZ introduced by offsetting caused an onion-ring structure.
(3) Sharp SiC particles from the AMC caused Fe debris from the steel pin, then transferred into the nugget zone during the FSW process, eventually leading to the forming of Al8Fe2Si particles during the FSW process.
(4) The tool offsetting showed little impact on the hardness values of the HAZ of the FSW joint, but slightly narrowed the HAZs due to the reduction of the flow of AMC into the NZ. The offset value did not have a significant effect on the overall strength of the FSW joint, as the fracture of the FSW joint always happened within the HAZ of Al alloy side.

Disclosure statement

No potential conflict of interest was reported by the author(s).

Funding

This work was supported by the Program for Guangdong Basic and Applied Basic Research Foundation [No. 2019A1515110525], the Liaoning Province Excellent Youth Foundation [No. 2021-YQ-01], Guangdong Introducing Innovative and Enterpreneurial Teams [No. 2016ZT06G025], and the Open Research Fund from the State Key Laboratory of Rolling and Automation, Northeastern University [2020RALKFKT009].

References

[1] Zhu SZ, Ma GN, Wang D, et al. Suppressed negative influence of natural aging in SiCp/6092Al composites. Mater Sci Eng A. 2019;767:138422.
[2] Mohammed IAR, Anwar K. Characterization of Al-7075 metal matrix composites: a review. J Mater Res Technol. 2019;8:3347–3356.
[3] Ureña A, Gómez de Salazar JM, Escalera MD. Influence of metal-ceramic interfaces on the behaviour of metal matrix composites and their joints. Key Eng Mater. 1996;127–131:687–694.
[4] Gómez de Salazar JM, Soria A, Barrena MI. Welding of AA6061-(Al2O3)p composite: effect of weld process variables and post-welding heat treatment on microstructure and mechanical properties. Sci Technol Weld Join. 2005;10:339–343.
[5] Mishra RS, Ma ZY. Friction stir welding and processing. Mater Sci Eng R. 2005;50:1–78.
[6] Nima SA, Seyyed EM, Kamran D. Effect of TiO_2 nanoparticles addition on microstructure and mechanical properties of dissimilar friction stir welded AA6063-T4 aluminum alloy and AZ31B-O magnesium alloy. J Manuf Process. 2019;38:338–354.
[7] Yang CL, Wu CS, Lv XQ. Numerical analysis of mass transfer and material mixing in friction stir welding of aluminum/magnesium alloys. J Manuf Process. 2018;32:380–394.
[8] Anaman SY, Cho H, Das H, et al. Microstructure and mechanical/electrochemical properties of friction stir butt welded joint of dissimilar aluminum and steel alloys. Mater Charact. 2019;154:67–79.
[9] Rzaev R, Chularis A, Smirnov V, et al. The influence of the friction stir welding parameters on the formation of welded joint of aluminum and copper alloys. Mater Today Proceed. 2019;11:534–542.
[10] Wert JA. Microstructures of friction stir weld joints between an aluminium-base metal matrix composite and a monolithic aluminium alloy. Scripta Mater. 2003;49:607–612.
[11] Guo J, Gougeon P, Chen XG. Microstructure evolution and mechanical properties of dissimilar friction stir welded joints between AA1100-B_4C MMC and AA6063 alloy. Mater Sci Eng A. 2012;553:149–156.
[12] Cioffi F, Ibáñez J, Fernández R, et al. The effect of lateral off-set on the tensile strength and fracture of dissimilar friction stir welds, 2024Al alloy and 17%SiC/2124Al composite. Mater Des. 2015;65:438–446.
[13] Xiao BL, Wang D, Bi J, et al. Friction stir welding of SiCp/Al composite and 2024Al alloy. Mater Sci Forum. 2010;638–642:1500–1505.
[14] Sharifitabar M, Nami H. Microstructures of dissimilar friction stir welded joints between 2024-T4 aluminum alloy and Al/Mg_2Si metal matrix cast composite. Compos B. 2011;42:2004–2012.

[15] Bai YF, Jiang XQ, Chen SJ, et al. Microstructure and properties of electrically assisted stationary shoulder friction stir welded Ti6Al4V. Sci Technol Weld Join. 2021;26:377–388.
[16] Sinhmar S, Dwivedi DK. Art of friction stir welding to produce weld joint without rotation of shoulder with narrow heat-affected zone and high corrosion resistance. Sci Technol Weld Join. 2020;25:490–495.
[17] Choi JW, Morisada Y, Liu HH, et al. Dissimilar friction stir welding of pure Ti and carbon fibre reinforced plastic. Sci Technol Weld Join. 2020;25:600–608.
[18] Feng AH, Xiao BL, Ma ZY. Effect of microstructural evolution on mechanical properties of friction stir welded AA2009/SiCp composite. Compos Sci Technol. 2008;68:2141–2148.
[19] Prado RA, Murr LE, Soto KF, et al. Self-optimization in tool wear for friction-stir welding of Al6061 + 20% Al_2O_3 MMC. Mater Sci Eng A. 2003;349:156–165.
[20] Fernandez GJ, Murr LE. Characterization of tool wear and weld optimization in the friction-stir welding of cast aluminum 359 + 20% SiC metal-matrix composite. Mater Charact. 2004;52:65–75.
[21] Shindo DJ, Rivera AR, Murr LE. Shape optimization for tool wear in the friction-stir welding of cast Al359-20%SiC MMC. J Mater Sci. 2002;37:4999–5005.
[22] Sharma N, Khan ZA, Siddiquee AN. Friction stir welding of aluminum to copper-an overview. Transf Nonfer Met Soc China. 2017;27:2113–2136.
[23] Shankar S, Vilaça P, Dash P, et al. Joint strength evaluation of friction stir welded Al-Cu dissimilar alloys. Measurement. 2019;146:892–902.
[24] Yasui T, Mizushima H, Tsubaki M, et al. Influence of tool shape on friction stir welded joint of aluminum and steel with circular weld line. Procedia Eng. 2014;81:2092–2097.
[25] Majeed T, Wahid MA, Alam MN, et al. Friction stir welding: a sustainable manufacturing process. Mater Today Proc. 2021;46:6558–6563.
[26] Sato YS, Kokawa H, Enomoto M, et al. Microstructural evolution of 6063 aluminum during friction-stir welding. Metall Mater Trans A. 1999;30:2429–2437.
[27] Ikeno S, Matsuda K, Rengakuji S, et al. Precipitation sequence in a SiC/Al-Mg_2Si alloy composite material. J Mater Sci. 2001;36:1921–1929.
[28] Nazari KA, Shabestari SG. Effect of micro alloying elements on the interfacial reactions between molten aluminum alloy and tool steel. J Alloy Compd. 2009;478:523–530.
[29] Kim B, Lee S, Lee S, et al. Real-time radiographic observation of solidification behavior of AlSiCu casting alloys with the variation of iron content. Mater Trans. 2012;53:374–379.
[30] Liu FC, Dong P. From thick intermetallic to nanoscale amorphous phase at Al-Fe joint interface: roles of friction stir welding conditions. Scripta Mater. 2021;191:167–172.
[31] Chang CI, Lee CJ, Huang JC. Relationship between grain size and Zener–Holloman parameter during friction stir processing in AZ31 Mg alloys. Scripta Mater. 2004;51:509–514.
[32] Heurtier P, Desrayaud C, Montheillet F. A thermomechanical analysis of the friction stir welding process. Mater Sci Forum. 2002;396–402:1537–1542.
[33] Feng AH, Ma ZY. Formation of Cu_2FeAl_7 phase in friction-stir-welded SiCp/Al-Cu-Mg composite. Scripta Mater. 2007;57:1113–1116.